Hydrogen Adsorption

DOI: 10.1002/anie.200604498

Manipulation and Patterning of the Surface Hydrogen Concentration on Pd(111) by Electric Fields**

Toshiyuki Mitsui, Evgeni Fomin, D. Frank Ogletree, Miquel Salmeron, Anand U. Nilekar, and Manos Mavrikakis*

Modification of the structure of materials at the nanoscale level is one goal of current nanoscience research. For example, by purposefully modifying the spatial distribution of adsorbates, the rate of chemical reactions could be controlled on a local scale. Herein, we show how this goal can be accomplished in the case of hydrogen on Pd(111) through the application of local electric fields. Hydrogen adsorption on the Group 10 metals is particularly interesting, because these metals are used as catalysts in a variety of industrial processes, including hydrogenation and dehydrogenation reactions.[1,2] Electric fields on surfaces are also of primary interest in electrochemistry,[3,4] and despite the considerable amount of experimental and theoretical work done to date,[5–12] there still remains more work to be done before a clear understanding of electric-field-induced phenomena at the atomic scale can be gained.

In a recent paper, Sykes et al.[13] describe the manipulation of H atoms on Pd(111) using the tip of a scanning tunneling microscope (STM). The authors propose that inelastic excitation by tunneling electrons drives H atoms from the bulk to the subsurface layers. Electronic excitations have also been shown to promote the selective desorption of H atoms from silicon.[14] Using a field ion microscope, Kellogg et al. found that strong electric fields enhance the diffusion of metal atoms towards the step edges that decorate the sharp tip.[15] Herein, we describe the manipulation of the concentration of surface hydrogen by means of electric fields which, as we will show using density functional theory (DFT) calculations, change the binding energy of surface and subsurface H atoms. Local electric fields drive hydrogen away from high-field regions of the surface and into subsurface layers.

The experiments were performed with a variable-temperature STM in ultra-high vacuum (UHV). The sample temperature could be varied from approximately 40 K to room temperature.[16] The Pd(111) crystal was cleaned by Ar-ion sputtering with subsequent annealing, then exposed to 10 L of hydrogen gas at 60–70 K, which produced a coverage between 0.75 and 1 monolayer (ML), as described previously.[17,18] Upon adsorption, H_2 molecules dissociate readily, and the H atoms occupy threefold face-centered cubic (fcc) sites, forming three ordered structures as a function of coverage: $(\sqrt{3}\times\sqrt{3})$ R30°–1H up to 0.33 ML, $(\sqrt{3}\times\sqrt{3})$ R30°–2H between 0.33 ML and 0.66 ML, and (1×1)–1H between 0.66 ML and 1 ML. In practice, it is difficult to reach coverage of 1 ML because of a significant reduction in the H_2 sticking coefficient with increasing coverage. Indeed, the STM images always show the presence of numerous residual vacancies. This finding reflects the fact that H_2 dissociation occurs preferentially at Pd atoms with no adjacent H atoms. These sites are only found when three or more vacancies coalesce.[19]

Under typical imaging conditions of 50–200 mV bias and 1–15 nA current, H atoms are imaged as depressions of approximately 5 pm, while H-atom vacancies give rise to protrusions of approximately 50 pm. With the same tunneling parameters, the average tip height during imaging is lowest (closer to the surface) for the (1×1)–1H structure, higher for the $(\sqrt{3}\times\sqrt{3})$ R30°–2H, higher yet for the $(\sqrt{3}\times\sqrt{3})$ R30°–1H, and highest for the clean surface. Since a linear gray scale is used to represent heights in the figures, it is easy to identify regions of low H-atom concentration in large images by their bright appearance, while high-concentration areas appear dark.

The manipulation experiments were performed on a nearly H-atom-saturated surface at temperatures between 40 K and 90 K. In Figure 1a, the tip was positioned near the image center, feedback control was disabled, and the bias voltage was increased from its imaging value of 70 mV to the manipulation value of 2 V for 10 milliseconds. After restoring the imaging parameters (15 nA, 70 mV), a new image was acquired (Figure 1b). As can be seen, the voltage pulse resulted in the formation of a roughly triangular patch with higher contrast (bright, because of reduced H-atom coverage) centered at the projected position of the tip during the pulse. The triangular patch is surrounded by a dark region with sixfold symmetry. Repeating the same experiment for increasingly long times gave rise to brighter and larger triangles surrounded by dark regions (Figure 1c–e). The size of the triangular region reached its maximum at around 30 nm

[*] Dr. T. Mitsui, Dr. E. Fomin, Dr. D. F. Ogletree, Dr. M. Salmeron
Lawrence Berkeley National Laboratory
Berkeley, CA 94720 (USA)
Fax: (+1) 510-486-6044
E-mail: mbsalmeron@lbl.gov
A. U. Nilekar, Prof. M. Mavrikakis
Department of Chemical & Biological Engineering
University of Wisconsin-Madison
Madison, WI 53706 (USA)

[**] Work at LBL was supported by the Director, Office of Energy Research, Office of Basic Energy Sciences, Materials Sciences Division of the U.S. Department of Energy under contract No. DE-AC02-05CH11231. Work at UW was supported by DOE-BES, Division of Chemical Sciences, under contract No. DE-FG02-05ER15731. A.U.N. and M.M. thank SC Johnson & Son, Inc. for a Distinguished Fellowship, and Drs. F. Mehmood, J. Rossmeisl, and Y. Xu for useful discussions. Computational resources at DOE-NERSC, PNNL, and ORNL are gratefully acknowledged.

Supporting information for this article is available on the WWW under http://www.angewandte.org or from the author.

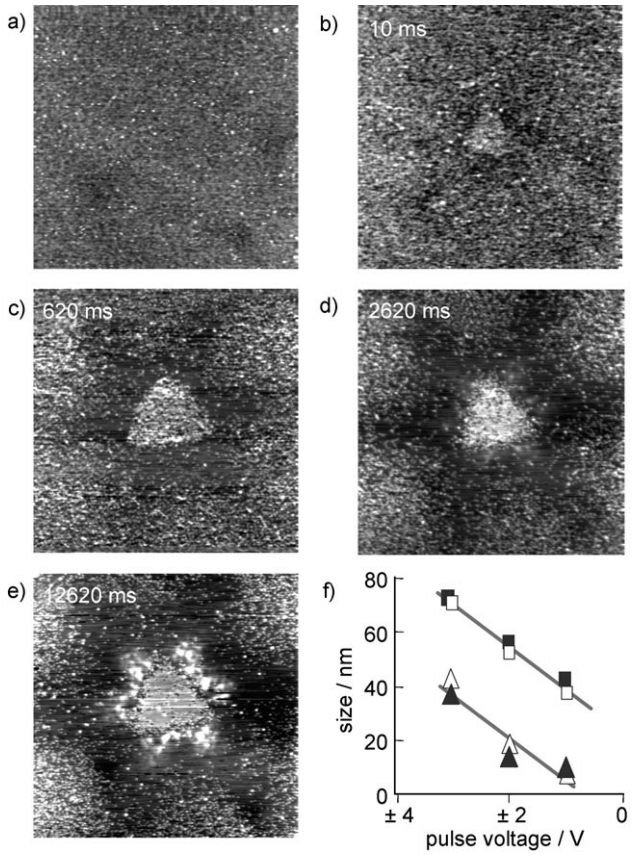

Figure 1. 100×100 nm² STM images of Pd(111) at 60 K (2 nA, 200 mV, tip–sample distance 0.5–0.7 nm) after an exposure to H_2 that produced a coverage close to one monolayer: a) before application of a voltage pulse; b) after a 10-ms 2-V pulse with the tip at the center; c) after an additional 610-ms pulse; d) after an additional 2000-ms pulse; e) after an additional 10-s pulse. Bright regions correspond to low H-atom coverage, while dark regions represent high coverage. The high electric field near the tip apex during the pulse drives hydrogen out of the central region, thus producing a roughly triangular region depleted of H atoms (brighter in the images). f) Lateral size of the hydrogen-depleted triangular region created by a 10-s pulse as a function of voltage (filled symbols represent negative pulses, open symbols represent positive pulses). The bottom curve (triangular symbols) was obtained with the tip approximately 0.2 nm closer to the surface than for the top curve (square symbols).

after a cumulative pulse length of 500 ms. Longer pulses (or a large number of short pulses in the same spot) resulted in the formation of additional bright satellite spots with sixfold symmetry located outside the triangle, as shown in Figure 1e after an accumulated 12.6-s pulse. The sides of the triangle are parallel to $\{1\bar{1}0\}$ directions. The effect of electric-field intensity was explored by increasing the voltage and by decreasing the distance of the tip to the surface. The linear dimensions of the pattern increased with field strength, as shown in Figure 1f, where the side length of the triangle produced by a 10-s pulse is plotted versus voltage for two different tip–surface separations. From the ratio of gap resistances during tunneling conditions (12.5 MΩ/100 MΩ), we calculated the tip–surface separation to decrease by about 0.2 nm from the lower to the upper curve (Figure 1f). Longer duration pulses or higher voltages produce a more rounded shape of the hydrogen-depleted regions in addition to the bright satellite spots surrounding the triangle in a sixfold symmetric pattern, as shown in Figure 1e. For voltages below 3 V, the results were independent of bias sign.

The atomic structure inside the triangles was $(\sqrt{3}\times\sqrt{3})$R30°–1H, $(\sqrt{3}\times\sqrt{3})$R30°–2H, or a mixture of both (Figure 2a). In the darker regions surrounding the triangle,

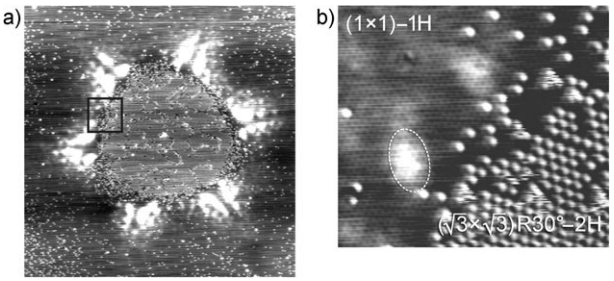

Figure 2. a) 60×60 nm² STM image of a hydrogen-covered Pd(111) surface (2 nA, 200 mV) 90 s after application of a 3-V pulse for 10 s between tip (located at the center) and surface. A region with rounded edges depleted of hydrogen has been created. The internal structure is $(\sqrt{3}\times\sqrt{3})$ R30°–2H (0.66 ML), with bright spots corresponding to H-atom vacancies. b) Expanded view (11×11 nm²) of the area marked by a box in (a). The region outside the triangle is covered by hydrogen in a (1×1)–1H pattern. Brighter regions, like the one enclosed by an oval, are 60 to 100 pm higher than the surrounding darker regions. They are associated with a local coverage higher than 1 ML, with the additional hydrogen in the subsurface layer.

the structure is a nearly perfect (1×1), as shown in Figure 2b, which corresponds to the area in the box in Figure 2a. The periodicity inside very bright regions decorating the triangles (like the one inside the dashed circle) is also (1×1), but these regions are approximately 60 pm higher than the surrounding area. The increased height in these regions is attributed to the expansion of the Pd interlayer spacing, which is due to H atoms below the surface, as discussed below.

The patterns generated by the voltage pulses can be explained as a result of redistribution of hydrogen induced by the electric field. The quasi-triangular symmetry of the H-atom-depleted regions can be explained by the directionality of the diffusion events. Previously, we have shown that hydrogen diffusion over bridge sites that are not adjacent to H-atom-occupied sites is much more favorable than diffusion over top sites, which gave rise to triangular aggregates of vacancies with sides aligned in $\{1\bar{1}0\}$ directions.[17,18] The diffusion of hydrogen away from the central region under the tip generates a concentration gradient with spots of high H-atom concentration that drives hydrogen to diffuse under the surface. As discussed below, the electric field affects the hydrogen binding energy. Since energy affects both equilibrium and kinetics in an exponential way, the electric field effects also decrease exponentially away from the tip apex projection. For that reason, unless the tip is very flat, only the atomic structure near the apex is important, which explains the symmetric structure of the hydrogen-concentration patterns. As the wave of H atoms diffusing away from the center abruptly slows down, it gives rise to spots of high concen-

tration. It is in these high-concentration spots, we think, that hydrogen diffuses into the bulk, producing the bright patches that surround the triangular hydrogen-depleted regions. The triangular features of reduced H-atom density slowly decay over tens of minutes at 40–60 K as hydrogen diffuses back into the depleted zone. Interestingly, the triangular outline is still recognizable during most of this process, since the H-atom diffusion within the border is much faster than across the border because of the lower hydrogen density.

An interesting characteristic of the hydrogen patterns is that they are "erasable" by electric fields. Figure 3a shows a roughly triangular region produced by a 2-V pulse. A second pulse was subsequently applied in the position marked by the arrow. As shown in Figure 3b, a new triangular region is produced, effectively erasing the previous one. A few bright spots are numbered in the images for reference. The patterning capabilities of this method are illustrated in Figure 3c, which was obtained with a multiasperity tip (such blunt tips are sometimes produced after mechanical contact with the sample). A triangular hydrogen-depleted region is produced at the projected position of each minitip.

To explain these observations, we performed self-consistent DFT calculations[20] using DACAPO[21] and determined the binding energy of atomic hydrogen (BE_H) as a function of coverage and electric field strength. The results of our calculations are shown in Figure 4, where the average binding energy BE_H of a H atom is plotted as a function of electric field strength for various coverages (θ_H). For each value of θ_H, the absolute value of BE_H is maximum at zero electric field and decreases with increasing field strength. As shown in the Supporting Information, for hydrogen coverage less than or equal to 1 ML, this destabilization originates from the lack of dipole-moment differences and polarizability differences between clean Pd and hydrogen-covered Pd in combination with the polarizability of gas-phase hydrogen. The latter factor accounts for the observed decrease in the average BE_H. In turn, this destabilization provides the thermodynamic driving force for the surface diffusion of hydrogen away from the tip, where the electric field is high, towards regions where the field is low. For coverages higher than 1 ML, population of subsurface sites leads to a significant charge redistribution near the surface, with a concomitant significant increase in the field-induced dipole. This effect tends to stabilize adsorbed hydrogen, partially offsetting the polarizability-related destabilization effect (for more details, see the Supporting Information). The complex interplay between field-induced dipole and polarizability effects, which vary with coverage and electric field strength, are responsible for the binding-energy features shown in Figure 4.

Figure 4 also shows that as θ_H increases, BE_H decreases, reflecting the repulsive interaction between coadsorbed H atoms. Interestingly, as mentioned above, at $\theta_H = 4/3$ ML the presence of 1/3 ML of hydrogen in the subsurface layer appears to stabilize the H atoms at higher positive electric fields. This effect further supports the model proposed above in which the bright broad spots in the images near the periphery of the hydrogen-depleted islands correspond to regions of subsurface H atoms. The electric field has therefore the dual effect of: 1) driving hydrogen away from the high-field regions, thereby increasing the concentration in the periphery; and 2) stabilizing subsurface hydrogen states. Unfortunately, the precise value of the electric field in the experiments can only be estimated, owing to incomplete knowledge of the tip shape and tip–surface distance. Simple

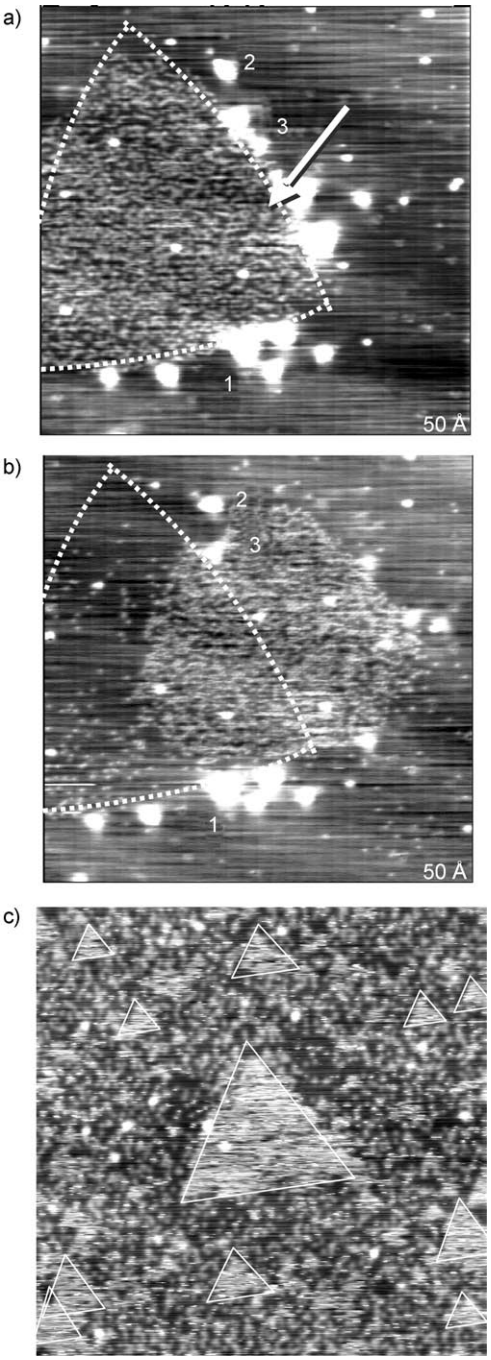

Figure 3. a) 50×50 nm² STM image ($T = 86$ K) showing a triangular region of depleted hydrogen after application of a 2-V pulse for 10 s. b) Same region after a second pulse at the position marked by the arrow in (a). Dashed lines mark the position of the initial triangle. The electric field redistributes hydrogen, "erasing" the original triangle and "writing" a new one. Bright protrusions are marked for reference. c) Multiple hydrogen-depleted triangles produced by a 2-V pulse using a multiasperity tip.

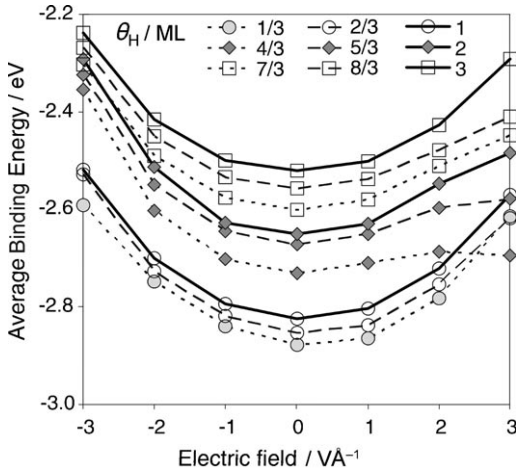

Figure 4. Calculated average binding energy of hydrogen on Pd(111) at various coverages from 1/3 to 3 ML, for a range of electric fields. Coverages above 1 ML correspond to hydrogen filling subsurface sites.

division of voltage (for 3 V) by tip–sample distance (ca. 5 Å) gives fields of about 0.6 V Å^{-1}, clearly smaller than the largest electric fields probed theoretically and displayed in Figure 4, however, the theoretically predicted trends are quite robust.

There are two other important results from the DFT calculations. One is that the projected density of states at the Fermi level as a function of coverage beyond 1 ML is essentially unchanged. The second is that there is an expansion of the Pd–Pd interlayer distance because of the presence of subsurface H atoms, resulting in an upward shift of the top Pd layer by 120 and 290 pm for 4/3 and 2 ML, respectively, relative to the full surface monolayer (1 ML) case. These results are in line with the contrast enhancement of the bright regions surrounding the triangles. The measured value of 60 pm is about half that predicted by the calculations, which might correspond to a lower concentration of subsurface hydrogen in the experiments. H-atom migration from surface to subsurface appears to be rather facile in Pd(111), as shown by our minimum-energy-path calculations[22] for diffusion of hydrogen on and into Pd(111), which yield activation energy barriers of 0.15 and 0.40 eV, respectively.[23]

In conclusion, our results show that electric fields are an important parameter that can affect adsorbate concentration and mobility on the surface of metal catalysts, including electrocatalysts. With the advent of modern developments in nanofabrication of addressable metal nanoelectrodes near surfaces,[24] the utilization of electric fields to generate specific patterns and reactivities on surfaces of interest can be envisioned.

Methods Section

A five-layer slab and a $(\sqrt{3}\times\sqrt{3})$R30° surface unit cell were periodically repeated in a supercell geometry with five equivalent layers of vacuum between successive metal slabs. Adsorption was allowed on only one of the two surfaces exposed, and the electrostatic potential was adjusted accordingly.[25] The top three layers of the slab were allowed to relax. Ionic cores were described by ultrasoft pseudopotentials,[26] and the Kohn–Sham one-electron valence states were expanded in a basis of plane waves with kinetic energy below 25 Ry. The surface Brillouin zone was sampled at 18 special Chadi–Cohen **k**-points.[27] The exchange-correlation energy and potential were described by the generalized gradient approximation (GGA-PW91).[28,29] The self-consistent PW91 density was determined by iterative diagonalization of the Kohn–Sham Hamiltonian, Fermi population of the Kohn–Sham states ($k_B T = 0.1$ eV), and Pulay mixing of the resulting electronic density.[30] Energies were extrapolated to $k_B T = 0$ eV. The calculated bond energy for H_2(g) was 4.57 eV, in reasonable agreement with the experimental value of 4.52 eV at 298 K.[31] Homogeneous external electric fields were imposed in our periodic calculations, as recently demonstrated by Rossmeisl et al.[12] For each electric field, the total energies of the gas-phase species, the clean metal slab, and the slab with adsorbed species on or in it were used to calculate the respective binding energies. For each specific electric field, BE_H is referred to a gas phase H atom and clean Pd(111) slab at infinite separation from each other. The lattice constant of bulk Pd is calculated to be 0.399 nm, in good agreement with the experimental value of 0.389 nm.[32]

Received: November 3, 2006
Revised: April 19, 2007
Published online: June 22, 2007

Keywords: adsorption · diffusion · electric fields · hydrogen · palladium

[1] C. N. Satterfield, *Heterogeneous Catalysis in Industrial Practice*, 2nd ed., Krieger Pulishing Company, Malabar, **1996**.
[2] J. Greeley, M. Mavrikakis, *J. Phys. Chem. B* **2005**, *109*, 3460.
[3] *Handbook of Fuel Cells: Fundamentals, Technology, Applications*, Wiley, West Sussex, **2003**.
[4] J. Greeley, J. K. Norskov, L. A. Kibler, A. M. El-Aziz, D. M. Kolb, *ChemPhysChem* **2006**, *7*, 1032.
[5] S. Holloway, J. K. Norskov, *J. Electroanal. Chem.* **1984**, *161*, 193.
[6] P. S. Bagus, C. J. Nelin, W. Muller, M. R. Philpott, H. Seki, *Phys. Rev. Lett.* **1987**, *58*, 559.
[7] D. K. Lambert, *J. Chem. Phys.* **1991**, *94*, 6237.
[8] M. Head-Gordon, J. C. Tully, *Chem. Phys.* **1993**, *175*, 37.
[9] F. Illas, F. Mele, D. Curulla, A. Clotet, J. M. Ricart, *Electrochim. Acta* **1998**, *44*, 1213.
[10] M. T. M. Koper, R. A. van Santen, *J. Electroanal. Chem.* **1999**, *472*, 126.
[11] S. A. Wasileski, M. T. M. Koper, M. J. Weaver, *J. Am. Chem. Soc.* **2002**, *124*, 2796.
[12] J. Rossmeisl, J. K. Norskov, C. D. Taylor, M. J. Janik, M. Neurock, *J. Phys. Chem. B* **2006**, *110*, 21833.
[13] E. C. H. Sykes, L. C. Fernandez-Torres, S. U. Nanayakkara, B. A. Mantooth, R. M. Nevin, P. S. Weiss, *Proc. Natl. Acad. Sci. USA* **2005**, *102*, 17907.
[14] T. C. Shen, C. Wang, G. C. Abeln, J. R. Tucker, J. W. Lyding, P. Avouris, R. E. Walkup, *Science* **1995**, *268*, 1590.
[15] G. L. Kellogg, T. T. Tsong, P. Cowan, *Surf. Sci.* **1978**, *70*, 485.
[16] S. Behler, M. K. Rose, J. C. Dunphy, D. F. Ogletree, M. Salmeron, C. Chapelier, *Rev. Sci. Instrum.* **1997**, *68*, 2479.
[17] T. Mitsui, M. K. Rose, E. Fomin, D. F. Ogletree, M. Salmeron, *Surf. Sci.* **2003**, *540*, 5.
[18] T. Mitsui, M. K. Rose, E. Fomin, D. F. Ogletree, M. Salmeron, *Nature* **2003**, *422*, 705.
[19] N. Lopez, Z. Lodziana, F. Illas, M. Salmeron, *Phys. Rev. Lett.* **2004**, *93*.
[20] J. Greeley, J. K. Nørskov, M. Mavrikakis, *Annu. Rev. Phys. Chem.* **2002**, *53*, 319.
[21] B. Hammer, L. B. Hansen, J. K. Nørskov, *Phys. Rev. B* **1999**, *59*, 7413.

[22] G. Henkelman, H. Jónsson, *J. Chem. Phys.* **2000**, *113*, 9978.
[23] Minimum energy paths for diffusion were uniformly upshifted in energy in the presence of nonzero electric fields, but the corresponding diffusion barriers remain practically invariant in the presence of such fields.
[24] X. M. Yan, S. Kwon, A. M. Contreras, J. Bokor, G. A. Somorjai, *Nano Lett.* **2005**, *5*, 745.
[25] J. Neugebauer, M. Scheffler, *Phys. Rev. B* **1992**, *46*, 16067.
[26] D. Vanderbilt, *Phys. Rev. B* **1990**, *41*, 7892.
[27] D. J. Chadi, M. L. Cohen, *Phys. Rev. B* **1973**, *8*, 5747.
[28] J. P. Perdew, J. A. Chevary, S. H. Vosko, K. A. Jackson, M. R. Pederson, D. J. Singh, C. Fiolhais, *Phys. Rev. B* **1992**, *46*, 6671.
[29] J. A. White, D. M. Bird, *Phys. Rev. B* **1994**, *50*, 4954.
[30] G. Kresse, J. Furthmuller, *Comput. Mater. Sci.* **1996**, *6*, 15.
[31] D. R. Lide, *CRC Handbook of Chemistry and Physics*, 76th ed., CRC Press, New York, **1996**.
[32] N. W. Ashcroft, N. D. Mermin, *Solid State Physics*, *Vol. 1*, Saunders College, Orlando, FL, **1976**.

